

Assessing cathode–electrolyte interphases in batteries

Received: 24 May 2024

Accepted: 19 August 2024

Published online: 07 October 2024

 Check for updates

Jie Xiao ^{1,2}✉, Nicole Adelstein ³, Yujing Bi ¹, Wenjuan Bian⁴, Jordi Cabana ⁵, Corie L. Cobb ², Yi Cui ^{6,7}, Shen J. Dillon⁸, Marca M. Doeff ⁹, Saiful M. Islam¹⁰, Kevin Leung ¹¹, Mengya Li¹², Feng Lin ¹³, Jun Liu ^{1,2}, Hongmei Luo¹⁴, Amy C. Marschlok^{15,16}, Ying Shirley Meng ¹⁷, Yue Qi ¹⁸, Ritu Sahore¹², Kayla G. Sprenger¹⁹, Robert C. Tenent²⁰, Michael F. Toney ¹⁹, Wei Tong ⁹, Liwen F. Wan²¹, Chongmin Wang ¹, Stephen E. Weitzner²¹, Bingbin Wu ¹ & Yaobin Xu ¹

The cathode–electrolyte interphase plays a pivotal role in determining the usable capacity and cycling stability of electrochemical cells, yet it is overshadowed by its counterpart, the solid–electrolyte interphase. This is primarily due to the prevalence of side reactions, particularly at low potentials on the negative electrode, especially in state-of-the-art Li-ion batteries where the charge cutoff voltage is limited. However, as the quest for high-energy battery technologies intensifies, there is a pressing need to advance the study of cathode–electrolyte interphase properties. Here, we present a comprehensive approach to analyse the cathode–electrolyte interphase in battery systems. We underscore the importance of employing model cathode materials and coin cell protocols to establish baseline performance. Additionally, we delve into the factors behind the inconsistent and occasionally controversial findings related to the cathode–electrolyte interphase. We also address the challenges and opportunities in characterizing and simulating the cathode–electrolyte interphase, offering potential solutions to enhance its relevance to real-world applications.

Almost all electrode couples in electrochemical cells operate beyond the thermodynamic stability limits of electrolytes¹. In many cases, these cells are only able to operate because the reactions between the electrode and electrolyte form new phases (or interphases) at the electrode–electrolyte interface. The canonical example of this is the stable solid–electrolyte interphase (SEI) layer² formed on graphite anode surfaces that enabled the commercialization of Li-ion batteries. Although high-quality SEI and cathode–electrolyte interphase

(CEI) layers may share similarities in terms of their stability, structural density, low impedance, thickness and so on, in practice the desired attributes of CEI layers are highly dependent on the battery system and cathode chemistry. For example, a thin CEI layer is usually preferred for fast ion diffusion^{3–5}, whereas a denser CEI can help mitigate transition metal dissolution from cathode surfaces^{6,7}. A dense and thin CEI may be preferred in many scenarios. However, the constituents of the optimized CEI in batteries designed for fast charging will be different

¹Pacific Northwest National Laboratory, Richland, WA, USA. ²University of Washington, Seattle, WA, USA. ³San Francisco State University, San Francisco, CA, USA. ⁴Idaho National Laboratory, Idaho Falls, ID, USA. ⁵Argonne National Laboratory, Lemont, IL, USA. ⁶SLAC National Accelerator Laboratory, Menlo Park, CA, USA. ⁷Stanford University, Stanford, CA, USA. ⁸University of California Irvine, Irvine, CA, USA. ⁹Lawrence Berkeley National Laboratory, Berkeley, CA, USA. ¹⁰Jackson State University, Jackson, MS, USA. ¹¹Sandia National Laboratories, Albuquerque, NM, USA. ¹²Oak Ridge National Laboratory, Oak Ridge, TN, USA. ¹³Virginia Tech, Blacksburg, VA, USA. ¹⁴New Mexico State University, Las Cruces, NM, USA. ¹⁵Brookhaven National Laboratory, Upton, NY, USA. ¹⁶Stony Brook University, Stony Brook, NY, USA. ¹⁷University of Chicago, Chicago, IL, USA. ¹⁸Brown University, Providence, RI, USA. ¹⁹University of Colorado Boulder, Boulder, CO, USA. ²⁰National Renewable Energy Laboratory, Golden, CO, USA. ²¹Lawrence Livermore National Laboratory, Livermore, CA, USA. ✉e-mail: jie.xiao@pnnl.gov

from those for high-energy applications, even if the same electrodes are used. This is because usually various additives are used in different battery systems^{8,9}. Therefore, there is no universal CEI (or SEI) that can meet the performance demands across all applications.

Despite the above-mentioned importance, the CEI has not attracted as much attention as its SEI counterpart. The main reason for this is probably that, for batteries with cutoff voltages below 4.2 V, most carbonate-based electrolytes are stable on the cathode but decompose more aggressively at the anode due to the very low electrode potentials. Nevertheless, as the demand for high-energy batteries continues to grow, in addition to the exploration of new high-energy materials^{10,11}, it is important to increase the battery operation voltage appropriately, so more capacity and energy can be extracted from the same set of cathode materials in the cell and pack, assuming that their structure remains stable. At elevated voltages, a stable CEI layer becomes critical for both battery performance and the structural stability of the cathode itself. Similarly to the SEI, the CEI is generated through the decomposition of electrolytes, albeit at high voltages, creating a passive film on the cathode surface¹². The presence and nature of the CEI thus directly determine the reversibility and efficiency of ion transport, assuming that the SEI or the anode itself are not hindering the overall cell reactions and acting as key limiting factors. In addition to electrolyte recipes, cathode surface chemistry¹³, morphologies¹⁴ and electrode potential¹⁵ all profoundly impact CEI components and properties.

A full understanding of CEI formation and evolution at varied length and time scales, especially at high voltages, is still lacking in the battery community. Progress is urgently needed to better tune CEI properties at the atomic scale to further stabilize the electrochemical energy storage system. Here, we summarize the inconsistent descriptions of the CEI from the literature, propose essential conditions (modelling cathode materials and coin cell protocols) for assessing the CEI properly, analyse the solutions to stabilize the CEI at high voltage and address the challenges and opportunities in characterizing and simulating the CEI without ambiguity.

Inconsistent descriptions of CEI from the literature

Although there are already many publications focusing on the CEI, a clear consensus has yet to emerge, and a lack of understanding persists on how to design and control CEI layers at the molecular level. Some of the potential factors behind the inconsistent and sometimes controversial discoveries on CEI include but are not limited to the following.

Lack of model materials with controllable surface properties

Many cathode materials used for CEI studies are synthesized in different laboratories, leading to variations in particle size, morphology and even stoichiometry of the as-prepared materials^{16,17}. The higher surface area of smaller cathode particles intensifies side reactions and impacts CEI formation^{18–20}. Even when commercially sourced cathode materials—for example, $\text{LiNi}_x\text{Mn}_y\text{Co}_z\text{O}_2$ (NMC811: $x = 0.8, y = 0.1, z = 0.1$ in weight percentage)—are used, depending on the storage conditions, the surface chemistry of NMC811 changes considerably—for example, when exposed to air²¹. The markedly different surface and bulk properties of cathode materials often determine the observed electrochemical performance, making it hard to isolate the CEI's effect in the electrochemical cell. To study the CEI, the cathode structure itself needs to be stable so that CEI impacts on the cathode can be extracted for investigation.

Reliable design of electrochemical cells for operando characterization of CEI

Electrochemical cells designed for in situ characterization sometimes introduce a remarkable increase in cell impedance because of their markedly modified cell format²². It is not uncommon that the applied potential is far beyond that normally used to charge small cells. In miniaturized characterization cells, the increased physical distance

between cathode and anode is another contributor to the high impedance, particularly when a non-aqueous electrolyte is used. The physics of the operando experiments can require cell architecture to be compromised to a point where it becomes irrelevant to real-world operation conditions. For example, some synchrotron and transmission electron microscopy (TEM) techniques require high vacuum, meaning that non-volatile electrolytes and open cell design must be used. However, in reality the cathode surface is buried deeply inside an operating cell and thus the design of in situ electrochemical cells that approach the behaviour of cells designed for battery benchmarking is critical in determining if an observation is a common phenomenon in CEI or only exists in the specific conditions imposed by the operando experiment due to the idiosyncrasies of the design of such small-scale cells^{22,23}.

CEI derived from flooded electrolytes versus CEI formed in lean electrolytes

Most characterizations are conducted on materials in cells flooded with electrolyte, often at volumes an order of magnitude greater than practically used in real batteries²⁴. The notably higher amount of electrolyte in flooded cells facilitates CEI dissolution and reformation during cycling. Thus, CEI composition and thickness continuously change. These changes make the observed properties of the CEI poorly representative when it comes to real batteries, in which the CEI is derived from very lean electrolyte conditions. Lean electrolyte is defined as the amount of electrolyte usually used in commercial Li-ion batteries with specified capacity and/or energy density, $\sim 1.3\text{--}1.5\text{ g Ah}^{-1}$ of electrolyte-to-capacity ratio²⁵. In coin cells, due to the large 'dead volume' that needs to be filled, the electrolyte is usually flooded and often 20–30 times more than in practical batteries that have specified energy requirement.

Cell failure is not dominantly caused by the CEI if the cathode is coupled with a poor anode

The electrochemical performance of a cell is determined by the worst electrode including its interphase, assuming that separators and electrolyte are reasonably good and not the limiting step via impeded Li^+ transport. For the initial assessment of CEI, half cells using Li metal as the counter-electrode will provide useful information, especially in the early stage of electrochemical reactions. Upon cycling, however, the Li metal anode itself becomes unstable due to the formation of mossy/dendritic Li. Cell impedance increases markedly and dominates the instability of performance. To fully understand the CEI and its evolution, especially after extensive cycling, a stable anode and its SEI are prerequisites. Many of the published papers studying the CEI or cathode still use Li metal as the anode to evaluate the cycling stability of the cathode, which is not relevant once Li metal degradation controls the cell performance. Full cells using stable graphite (and stable SEI) as the anode are necessary to ensure that the electrochemical reaction is mainly controlled by the CEI during extensive cycling, thereby enabling an accurate interpretation of the electrochemical data.

Assessing CEI in relevant conditions

Full-coin-cell protocols to ensure that the CEI dictates the macroscopic performance: one prerequisite to understand and address CEI challenges at high voltages is to ensure that the interfacial phenomena captured between cathode and electrolyte not only occur in practical batteries, but also play a dominant role in the electrochemical performance. This is because the performance of any electrochemical cell is dictated by the slowest step or worst component during battery operation²⁶. If the observed electrochemical performance is not dominated by the CEI, it is challenging to assess the utility of CEI engineering efforts, since the impact of CEI properties on cell performance is masked by extraneous limiting factors.

Similarly, a stable anode such as graphite is necessary to effectively evaluate CEI and cathode behaviours. If Li metal is used as the

Table 1 | Full-coin-cell parameters in the standard testing protocol developed at Pacific Northwest National Laboratory. Data from ref. 89

Cathode: NMC811 (polycrystals or single crystals)	
Active material	96 wt%
Carbon	2 wt%
Polyvinylidene difluoride	2 wt%
Mass loading (NMC only)	~15 mg cm ⁻²
Specific capacity	~200 mAh g ⁻¹ (C/10)
Areal capacity	~3 mAh cm ⁻²
Voltage window	2.6–4.3 V versus Gr (2.7–4.4 V versus Li)
Porosity	~35%
Graphite anode	
Areal capacity	3.6 mAh cm ⁻²
Porosity	40–45%
Negative/positive ratio	~1.2
Baseline electrolyte	1M LiPF ₆ in EC/EMC (3:7)+2% VC
Formation cycle	C/10 for charge & discharge for three cycles
Charge	CC-CV: C/3 to 4.3 V (versus Gr) then constant voltage until $I \leq C/20$
Discharge	C/3

Abbreviations: Gr, graphite; EC, ethylene carbonate; EMC, ethyl methyl carbonate; VC, vinylene carbonate; CC-CV, constant current and constant voltage; I , current.

counter-electrode, there are always excessive amounts of Li⁺ in the cell. However, in cells with graphite anodes, the Li inventory is restricted to that provided by the cathode. Therefore, the usable capacity of the cathode can be fully realized during the initial cycling, which is helpful for understanding its material properties. Nevertheless, coin cells using Li metal anodes help to design a balanced full cell with appropriate negative/positive ratios and have the added benefit of being simpler to assemble. The latter is highly useful for characterization purposes, especially for in situ or operando probing. Moreover, for small cycle numbers, the CEI of such half cells will not differ considerably from those in graphite-based full coin cells; however, their long-time cycling behaviour will mainly reflect Li metal problems instead of cathode/CEI stability²⁴. Thus, it is when the long-term stability of the CEI becomes the focus of study that coupling with a stable graphite anode is necessary to ensure that the sensitivity of the cell performance to the CEI is properly established.

While preferable for long-term CEI evaluation, graphite-based full cells, in contrast to Li metal half cells, have more parameters to control for to ensure reproducibility, from electrode coating to cell assembly and testing²⁷. Table 1 lists the necessary parameters to construct and test full coin cells under conditions that are relevant to practical batteries, while being suitable to evaluate the impact of CEI engineering solutions. A more detailed assembly process can be found in our previously published paper²⁷. Depending on the intended application, the areal loading and porosity of the cathode (and anode) in Table 1 can be further tuned for high-energy, high-power or fast-charging systems.

As mentioned earlier, another issue with using a coin cell as the testing vehicle is that the electrolyte, which must fill in all the void spaces in the device, is in large excess when compared with that in pouch cells. This fact adds some uncertainty to the study of the CEI dissolution in coin cells, given the flooding by the electrolyte, which may dissolve some of the CEI components such as LiF or Li₂CO₃. Therefore, ultimately, a pouch cell with targeted capacity, energy or power is the best platform for cross-validation. Because they are simpler to assemble, the full-coin-cell protocol listed in Table 1 should be

viewed as a powerful vehicle to quickly identify the most valuable approaches, ensure fair and consistent comparisons and provide a gateway for further implementation of new materials in full-format pouch cells.

Model cathode materials to investigate CEI at high voltages

Cathode stability at high voltages is impacted by both the interfacial and bulk properties of the material. Therefore, a model cathode material that does not undergo notable structural change at high voltages will be critical to explore CEI formation and evolution. Single-crystal Ni-rich NMC is a good example of a model material for this purpose. For example, single-crystal Ni-rich NMC prepared using a molten salt approach¹⁵ (Fig. 1a–c) has controlled morphologies that can be used for various purposes. Cylinder-shaped (Fig. 1a) or drum-like NMC76 ($x = 0.76, y = 0.14, z = 0.1$) (Fig. 1b) single crystals expose different facets to the liquid electrolyte, providing a unique opportunity to study prepared CEI formation or decomposition, if any, on specific lattice planes. Single crystals of NMC76 can also grow as large as ~30 μm in diameter (Fig. 1c) and still display electrochemical activity, albeit at a very slow rate (Fig. 1g), rendering them a perfect platform for operando characterization of CEI in a ‘living’ electrochemical cell. Irregularly shaped NMC811 single crystals (Fig. 1d) developed from solid-state synthesis²⁸ provide a good comparison with those formed on crystals grown from molten salts, as the surface properties and impurity levels are quite different from the beginning of processing. For each model cathode, a baseline performance derived from full coin cells using the corresponding protocols will be critical to benchmark future results.

Commercial polycrystalline NMC811 is also a good model material to establish convincing baseline performance when compared with laboratory-made cathode materials, using similar cell parameters and testing conditions. Unfortunately, it is not uncommon in the literature to use poorly performing and poorly characterized cathodes as controls to misleadingly claim an improvement of modified materials, which is detrimental to advancing technology development. Figure 2 is an example of coin cell performances that can be used as a baseline for NMC (or graphite) research. The NMC811 cathode and graphite anode are both from commercial sources. The electrolyte used is the same baseline electrolyte as listed in Table 1. Electrodes are constructed corresponding to the key parameters in Table 1. It is clear that, between 2.6 and 4.2 V, very stable cycling is achievable from graphite/NMC811 coin cells without modifying electrodes or using any additives. Even when the cutoff voltage is increased to 4.3 V (versus graphite), the full coin cell still demonstrated good cycling stability, with 82.7% capacity retention after 500 cycles, similar to the cells cycled between 2.6 and 4.2 V.

In fact, any of the cathode materials can be used as a model material to study the CEI or its own structural stability, provided that the cathode and CEI are the controlling factors determining the cell performance. Upon establishment of baseline performance, CEI improvements achieved via surface coating or electrolyte reformulation will become rational and reproducible. However, for materials exhibiting extraordinary CEI stability at the materials level, implementations at the particle level with high mass loading and controlled porosity remain challenging^{29,30}.

Stabilizing CEI at high voltages High-voltage operation of Li-ion batteries

To stabilize the CEI at high voltages, it is first necessary to define how high a cutoff must be reached in an electric vehicle battery based on Li-ion chemistry. For illustration, Table 2 compares the capacity and energy gain, as well as the reduction of a critical element such as cobalt, in a 100 kWh electric vehicle battery pack adopting graphite/NMC chemistry charged to various cutoff voltages.

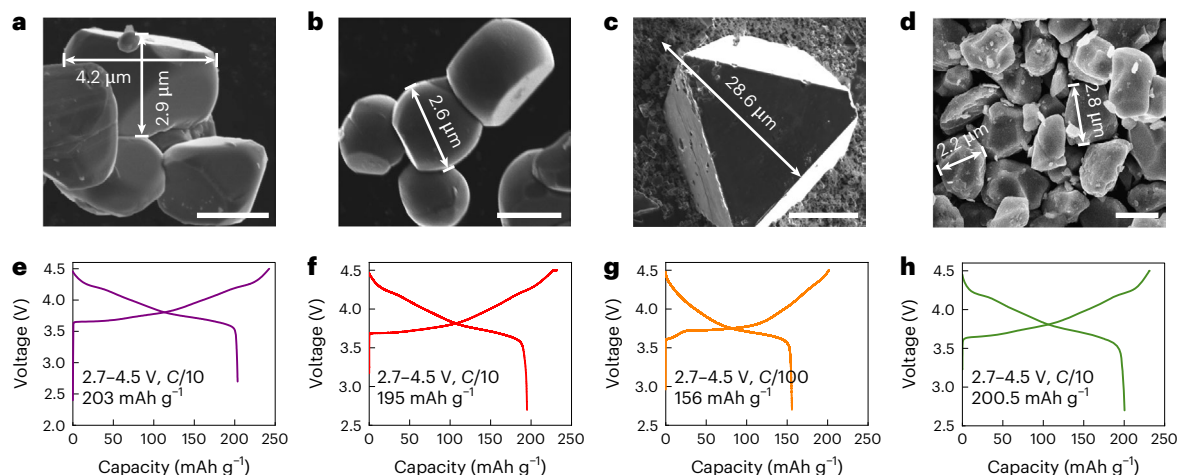


Fig. 1 | Single-crystal Ni-rich NMC with different morphologies as model materials. **a**, Single-crystal NMC76 with an average crystal size of 3–4 μm (ref. 89). **b**, Modified single-crystal NMC76 with drum-like morphology⁸⁹. **c**, Approximately 30-μm-diameter single-crystal NMC76 with (001) and (012) planes exposed, ideal for in situ characterizations⁸⁹. **d**, Single-crystal NMC811 with irregular morphology⁸⁹. **e**, The charge–discharge curve of single-crystal NMC76 in **a**. 203 mAh g⁻¹ capacity is delivered when charged to 4.5 V versus Li/Li⁺ (ref. 89). **f**, The charge–discharge curve of drum-like single crystals in **b**. 195 mAh g⁻¹ capacity is delivered when charged to 4.5 V versus Li/Li⁺ (ref. 89).

g, The charge–discharge curve of the 20 μm single crystal in **c**⁸⁹. At a very slow rate of C/100, 156 mAh g⁻¹ capacity is still delivered from such a huge crystal when charged to 4.5 V versus Li/Li⁺. **h**, The charge–discharge curve of the approximately 2 μm single crystal in **d**⁸⁹. 202 mAh g⁻¹ capacity is obtained when charged to 4.5 V versus Li/Li⁺. The crystals presented in **a–c** were synthesized using a molten salt approach¹⁵, while those in **d** were prepared by a solid-state synthesis⁹⁰. Figure reproduced from ref. 89, US DOE. Scale bars, 2 μm (**a–c**), 10 μm (**d**).

NMC811

The cutoff voltage is usually set to 4.2 V (versus graphite, corresponding to 4.3 V versus Li/Li⁺) for commercial Li-ion batteries. If charged to 4.3 V versus graphite, the usable discharge capacity of NMC811 is increased from 190 mAh g⁻¹ (at 4.2 V versus graphite) to 210 mAh g⁻¹, accompanied by a slightly increased average discharge voltage. The capacity gain of 20 mAh g⁻¹ simply by raising the cutoff voltage effectively increases cell-level energy and provides more needed flexibility for the cell-level design. For the same 100 kWh pack, increasing the cutoff voltage from 4.2 to 4.3 V also means that less cathode material may be needed to meet an energy target, reducing battery pack weight by 17 kg and the amount of cobalt by 1 kg. Further increasing the cutoff voltage of the Gr/NMC811 couple to 4.4 V extracts a capacity that is slightly higher, by 5 mAh g⁻¹, but the advantages become limited (Table 2). It is probably not worthwhile to increase the upper limit by 100 mV because of the very strict requirements for solvent purity and anodic stability. Usually, the entire electrochemical stability window of the electrolyte shifts towards either higher or lower potentials in the same direction. Expanding the window towards both high and low voltage ranges simultaneously is quite challenging. Consequently, the electrolyte that stabilizes the CEI at very high voltages beyond 4.3 V could easily become unstable with respect to the anode. Additionally, Ni-rich NMCs are not stable beyond 4.3 V (versus graphite) due to phase transitions and increased probability of gas evolution. Therefore, developing a functional electrolyte that ensures a stable CEI above 4.3 V (versus graphite) may not be useful, unless the structural instability of NMC811 itself is addressed first.

Beyond NMC811

NMC with very high Ni content—for example, NMC95 ($x = 0.95, y = 0.04, z = 0.01$)—is only stable to 4.04 V versus graphite³¹. Aggressive side reactions occur between the cathode surface and the electrolyte even at 4.18 V (versus graphite), which is reflected by the continuous cathode impedance growth upon cycling. Therefore, the definition of ‘high’ voltage depends on cathode composition and may differ from that for cells containing NMC811. In this case, stabilizing Ni-rich NMC below 4.3 V (versus graphite) or 4.4 V (versus Li/Li⁺) is sufficient to balance energy

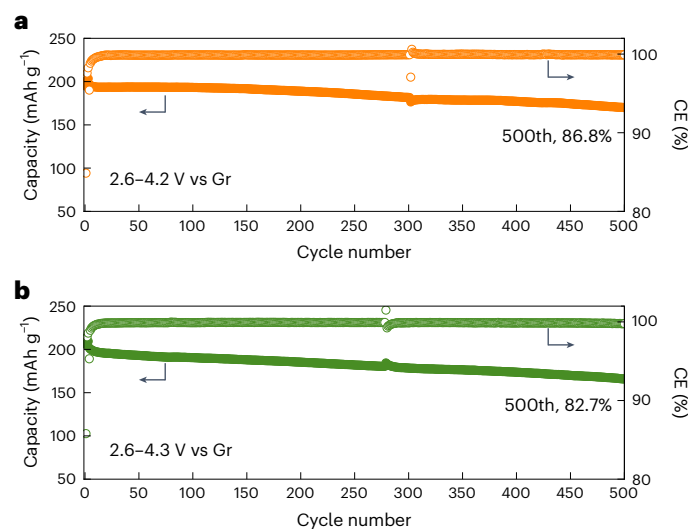


Fig. 2 | Electrochemical performance of NMC811 polycrystals tested in full coin cells that use graphite as anode. **a**, Cycling performance of NMC811 tested between 2.6 and 4.2 V versus graphite. **b**, Cycling performance of NMC811 tested between 2.6 and 4.3 V versus graphite. Commercial NMC811 cathode and graphite anode materials are used in this full-coin-cell testing with the protocols listed in Table 1. Baseline electrolyte, that is, 1 M LiPF₆ in EC/EMC + 2% VC, is used for coin cell testing. C/3 was used for both charge and discharge after three formation cycles at C/10. 1 C was defined as 200 mA g⁻¹. These performances can be used as baseline performances to benchmark any further modification on the cathode, anode or electrolyte. Figure reproduced from ref. 89, US DOE.

gain and cycling stability. For example, for NMC90 ($x = 0.9, y = 0.05, z = 0.05$), the charge cutoff voltage that enables stable cycling may reside between 4.1 and 4.2 V and requires further study. The amount of cobalt in the same 100 kWh electric vehicle pack using NMC90 is reduced by half while providing more energy with less battery weight (Table 2). The problem with NMC90 is that, even if the electrochemical window is limited to 2.6–4.2 V (versus graphite), its stability is already

Table 2 | Usable capacity and energy from NMC811 charged to different voltages in a 100 kWh Li-ion battery pack

Material	Voltage window (V)	Usable capacity (mAhg ⁻¹)	Average discharge voltage (V)	Material energy (Whkg ⁻¹)	Total NMC mass in 100 kWh LIB pack (kg)	Cobalt mass (kg)
NMC811	2.7–4.1	180	3.60	648	154	9.3
	2.7–4.2	190	3.65	694	144	8.7
	2.7–4.3	199	3.70	736	136	8.2
	2.7–4.4	204	3.70	759	132	8.0
NMC90	2.7–4.1	185	3.69	683	146	4.4
	2.7–4.2	195	3.73	727	137	4.2
	2.7–4.3	204	3.76	767	130	3.9
	2.7–4.4	212	3.78	803	125	3.8

Voltage refers to the value versus graphite, and capacity is obtained at C/3 rate. These data are for illustrative purposes. Abbreviation: LIB, lithium-ion battery.

worse than NMC811 cycled within the same voltage range due to the unstable Ni-rich surface and severe growth of impedance upon cycling. This fact makes pushing the cutoff voltage to 4.3 V a daunting endeavour at the current time. Thermal stability is another concern if the Ni content is too high in NMC. Single-crystal morphologies may help stabilize NMC811 and NMC90 at elevated potentials, but more work is still needed to confirm this promise. In addition to morphology control, for NMC90 (or compositions with even higher Ni content), stable electrolytes that are resistant to highly active O, suppress cathode impedance growth and enhance the thermal stability of the cathode need to be identified to unlock their full potential. Optimization of Ni content in NMC with an electrochemical window that matches currently available functional electrolytes may also provide a means to balance the energy, cycle life and safety of Li-ion batteries employing high-Ni-content NMCs as cathodes.

Electrolytes and additives to stabilize CEI

The CEI builds up from decomposition by-products of the electrolyte on the cathode particle surfaces. Therefore, the electrolyte constituents and their relative stability during polarization largely determine the CEI components. The effective evaluation of electrolytes and their derived CEI layers is built upon a few assumptions, including but not limited to the following: (1) the cathode itself is free of pre-existing surface impurities left over from synthesis³² or developed during storage²¹, (2) the electrolyte has no residual water or other impurities that will detrimentally affect the cell performance³³ and (3) there is no migration of transition metal cations from the cathode to the anode, which may damage the SEI, causing fast cell degradation. The crosstalk of cathode and anode mainly impacts the SEI on the anode side triggered by metal cation migrations, especially for high-voltage cathode materials (4.5–4.6 V)³⁴ or a Si/graphite anode³⁵.

Electrochemically, the CEI (or SEI) formation processes are closely related to the components within the electrical double layers³⁶ developed in the vicinity of the electrode before any electrochemical or side reactions start (Fig. 3). Before charge transfer takes place, anions adsorb on the positively charged cathode material surface (left side in Fig. 3) along with a small number of solvent molecules, forming an inner Helmholtz layer (IHL). As the positively charged surface continues to be polarized, these anions will be oxidized and converted to the CEI components. Solvent molecules within the IHL will also be oxidized, but unless they have a strong adsorption capability to the positive electrode or possess a very low energy barrier for oxidation the anions will always be initially oxidized within the IHL. Therefore, to tune the composition and properties of CEI layers, the addition of certain anions that will be preferentially oxidized during charging to form an enhanced inorganic layer for the CEI may be valuable. If certain

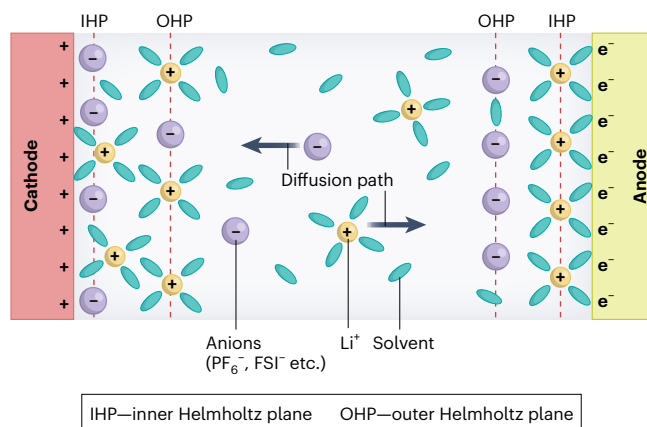


Fig. 3 | Electrical double layers formed on positive electrode (cathode in battery) and negative electrode sides (anode in battery) during charge process. The constituents in the IHL are related to the later formed passivation layers on positive and negative electrodes, which can be used to help develop better electrolytes or additives to tune CEI or SEI properties.

solvent additives that are known to help enhance CEI properties are used in the electrolyte, they need to have a strong adsorption ability on the positively charged electrode to fully unlock their potential to enhance CEI properties.

The relationship between the IHL and the passivation film formation process provides avenues to rationalize why concentrated electrolytes can be used to manipulate the CEI³⁷ (and SEI³⁸). As the concentration of Li salts increases, anions become more abundant in the IHLs of both positive and negative sides and, therefore, enhance the contribution of anion-derived inorganic components in the passive films formed on the electrodes. Note that the formation of the CEI (and SEI) depends on the Gibbs free energy difference between the reactants (electrolytes) and products after the electrochemical/chemical reactions³⁹. Some qualitative trends can be established by comparing the energies of the highest occupied molecular orbital and lowest unoccupied molecular orbital of different electrolyte components.

More evidence can be found in Table 3, which summarizes the functional electrolytes and additives that have been reported in the literature for use with Ni-rich cathodes. Here, we only consider the results for Ni-rich cathodes tested in full coin or pouch cells for the reasons we have discussed earlier. When the oxidation of Ni-rich materials intensifies at high potentials, conventional carbonates become thermodynamically unstable on their surfaces⁴⁰. EC plays a vital role in forming a stable SEI on graphite, but it undergoes notable decomposition concurrently at the cathode side and generates CO₂, CO and H₂O. These reactions are further aggravated in the presence of active oxygen released from Ni-rich NMC at elevated potentials⁴¹. EC-free electrolytes have been proposed to enhance the anodic stability on Ni-rich cathodes by incorporating multiple Li salts in linear carbonates⁴², which in fact tunes the anions within the cathode IHL. Solvents with great stability, such as sulfones⁴³, sulfonates⁴⁴, nitriles⁴⁵, fluorinated carbonates and ethers^{3,46–53}, are also proposed to enhance CEI properties. However, it is important to remark that the change of solvent molecules in the electrolyte can preferentially impact the SEI since solvents are the dominant species in the IHL of negative electrodes (Fig. 3). Therefore, any evaluation of solvent modification to enhance the CEI must eventually contend with evaluations of whether the quality of the SEI is, at least, not degraded, which demands further dedicated investigations. Decoupling the cathode and anode reactions is critical to understand which component is being impacted more importantly when even a small change is introduced into the cell⁵⁴.

Table 3 | Functional electrolytes for NMC811 in coin/pouch-type Li-ion batteries using graphite as the anode

Electrolyte recipes	Battery type	Working voltage (V versus Gr)	Cathode loading or areal capacity (mgcm ⁻² or mAhcm ⁻²)	Capacity retention	Charge/discharge rate	Ref.
Based on solvent change or mixing						
LiPF ₆ :MDFA:PFPN:FEC (1:7:0.5:1 by mol)	240mAh pouch cell	2.8–4.3	13.2	81.8%@500 cycles	1C/1C	46
1.0M LiPF ₆ :PC:TFA (3:7 by vol.)	730mAh pouch cell	2.7–4.3 (45 °C)	12.1	82%@400 cycles	1C/1C	47
1.6M LiFSI TEOSCN	1Ah pouch cell	2.8–4.3	N/A	95%@500 cycles	0.2C/0.2C	45
1.0M LiPF ₆ /0.02M LiDFOB FEC:HFE:FEMC (2:2:6 by vol.)	1Ah pouch cell	3–4.3	N/A (single-crystal 811 used)	110.1%@200 cycles	0.33C/0.33C	48
LiFSI:DMC:EC:TTE (1:4.8:0.2:1 by mol)	Coin cell	2.5–4.4	1.5mAhcm ⁻²	69%@300 cycles	4C/0.33C	3
1.0M LiPF ₆ :SL:FEC:EMC (1:1:3 by vol.)+0.5wt% LiBF ₄ /LiNO ₃	Coin cell	2.75–4.4	20	85.2%@300 cycles	0.5C/0.5C	43
1.0M LiPF ₆ in FEC:TTE (6:4 by vol.)	1Ah pouch cell	3–4.4	N/A	91%@300 cycles	1C/1C	49
LiFSI:DME:FEC:PFPN (1:1.5:0.5:3 by mol)	Coin cell	2.5–4.5	8.35	82%@1,000 cycles	0.33C/0.33C	50
1.0M LiTFSI MDFA:MDFSA:TTE (4:1:5 by mol)	Coin cell	2.5–4.5	11.5	80.1%@400 cycles	0.5C/0.5C	52
0.8M LiFSI–0.1M LiTFSI–0.6M LiPF ₆ EMC	1Ah pouch cell	3–4.5	13.5	82.1%@200 cycles	0.33C/0.33C	42
1.9M LiFSI TTMS:TM (1:2 by vol.)	1Ah pouch cell	3–4.6	N/A	83%@1,000 cycles	0.5C/1C	44
LiDFOB:MP:mFT:TTE (1:2.67:1:1 by mol)	1.2Ah pouch cell	2.8–4.6	17.4	90.4%@130 cycles	0.2C/0.2C	51
Based on anion change or mixing						
1.0M LiPF ₆ EC:EMC (3:7 by wt)+0.4wt% NaH ₂ PO ₄	Coin cell	3–4.3 (60 °C)	2.6mAhcm ⁻²	75%@150 cycles	0.5C/0.5C	56
1.0M LiPF ₆ EC:EMC (3:7 by vol.)+2wt% VC	200mAh pouch cell	2.8–4.4 (40 °C)	N/A	80%@200 cycles	0.2C/0.2C	55
1.0M LiPF ₆ EC:EMC (3:7 by vol.)+2wt% VC+2wt% LiDFOB+1wt% TMSPi	Coin cell	2.5–4.5	24	85%@300 cycles	0.2C/0.5C	60
1.0M LiPF ₆ EC:DEC (1:1 by vol.)+2wt% TMSP+0.1M LiDFOB	Single-layer pouch cell	2.7–4.5	N/A	82.8%@500 cycles	1C/1C	61
1.0M LiPF ₆ EC:EMC (1:2 by vol.)+1wt% DES	1.95Ah pouch cell	2.75–4.5	N/A	82.5%@150 cycles	1C/1C	58

Abbreviations: MDFA, methyl difluoroacetate; PFPN, ethoxy-pentafluoro-cyclotriphosphazene; FEC, fluoroethylene carbonate; PC, propylene carbonate; TFA, 2,2,2-trifluoroethyl acetate; TEOSCN, (2-cyanoethyl)triethoxysilane; LiDFOB, lithium difluoro(oxalato)borate; HFE, hydrofluoroether; FEMC, (2,2,2-trifluoroethyl) carbonate; DMC, dimethyl carbonate; EC, ethylene carbonate; TTE, 1,1,2,2-tetrafluoroethyl-2,2,3,3-tetrafluoropropyl ether; SL, sulfolane; EMC, ethyl methyl carbonate; PFPN, ethoxy(pentafluoro) cyclotriphosphazene; DME, dimethoxyethane; MDFA, methyl difluoroacetate; MDFSA, methyl 2,2-difluoro-2 (fluorosulfonyl)acetate; TTMS, 2,2,2-trifluoroethyl trifluoromethanesulfonate; TM, 2,2,2-trifluoroethyl methanesulfonate; MP, methyl propionate; mFT, m-fluorotoluene; VC, vinylene carbonate; TMSPi, tris(trimethylsilyl)phosphite; DEC, diethyl carbonate; TMSP, tris(trimethylsilyl)phosphate; DES, 3,3-diethylene di-sulfite.

To replace conventional EC-based electrolytes for Li-ion batteries, an overall assessment of large-full-cell performances including cycling stability, rate capability, low/high-temperature performance, shelf life and resistance to abuse is necessary. At the time of writing, additives in the form of either solvents or anions, rather than completely switching to a non-carbonate solvent, probably offer more viable pathways for practical applications. Additives that can kinetically form a robust CEI layer on the cathode and prevent further electrolyte decomposition at high voltages are also reported. Many of these additives, such as carbon⁵⁵, phosphorus⁵⁶, boron⁵⁷, sulfur⁵⁸ and nitrogen⁵⁹-based compounds, or their combinations^{60,61}, have been developed for cathode materials with relatively low Ni (Ni < 0.8) content (for example, NMC442^{62,63} or NMC532^{64,65}), but operating at voltages of ≥4.4 V (versus graphite). More full-cell work is needed to confirm the effectiveness of these previously explored additives for Ni-rich NMC (Ni ≥ 0.8) charged up to 4.4 V (versus graphite).

While different electrolyte recipes should be developed depending on the specific applications of Li-ion batteries, the unstable nature of Ni-rich surfaces is the root cause that has delayed the large-scale commercialization of high-Ni-content NMC, and therefore needs to be addressed first. In addition to the electrolyte itself, appropriate selection of doping elements or artificial coating layers on the cathode may also help to mitigate the electrolyte decomposition and gassing issues commonly found for Ni-rich cathodes.

Integrating characterization and modelling into assessing the CEI

Since the discovery of the existence of CEI layers on cathodes in the 1980s⁶⁶, there have been many advances in investigating their chemical composition, microstructure and electronic structure for Li-ion batteries and beyond.

To achieve a holistic understanding of the CEI without ambiguity, there is a critical need to develop advanced characterization techniques that are non-destructive, in situ/operando and that have high sensitivity, lateral/spatial/temporal resolution, throughput and automation attributes, and to further combine these with advanced multiscale modelling tools as shown in Fig. 4. Tool selection also needs to address the challenges associated with directly probing the dynamically evolving structure, chemistry and properties of the CEI. These challenges arise not only from the different chemical nature and operating conditions, but also from less controllable factors such as preparation route, porosity and surface morphology/impurities of the cathode architecture. For example, the surface native film (LiOH, Li₂CO₃) formed on an NMC cathode during synthesis, storage and assembly adds considerable complications to CEI formation and characterization. Model cathode materials with controllable surface properties are critical for CEI investigations with definitive results. Flooding of electrolytes will also introduce more interactions between the electrolyte, carbon black and binder as well as unlocking possible pathways of CEI redissolution,

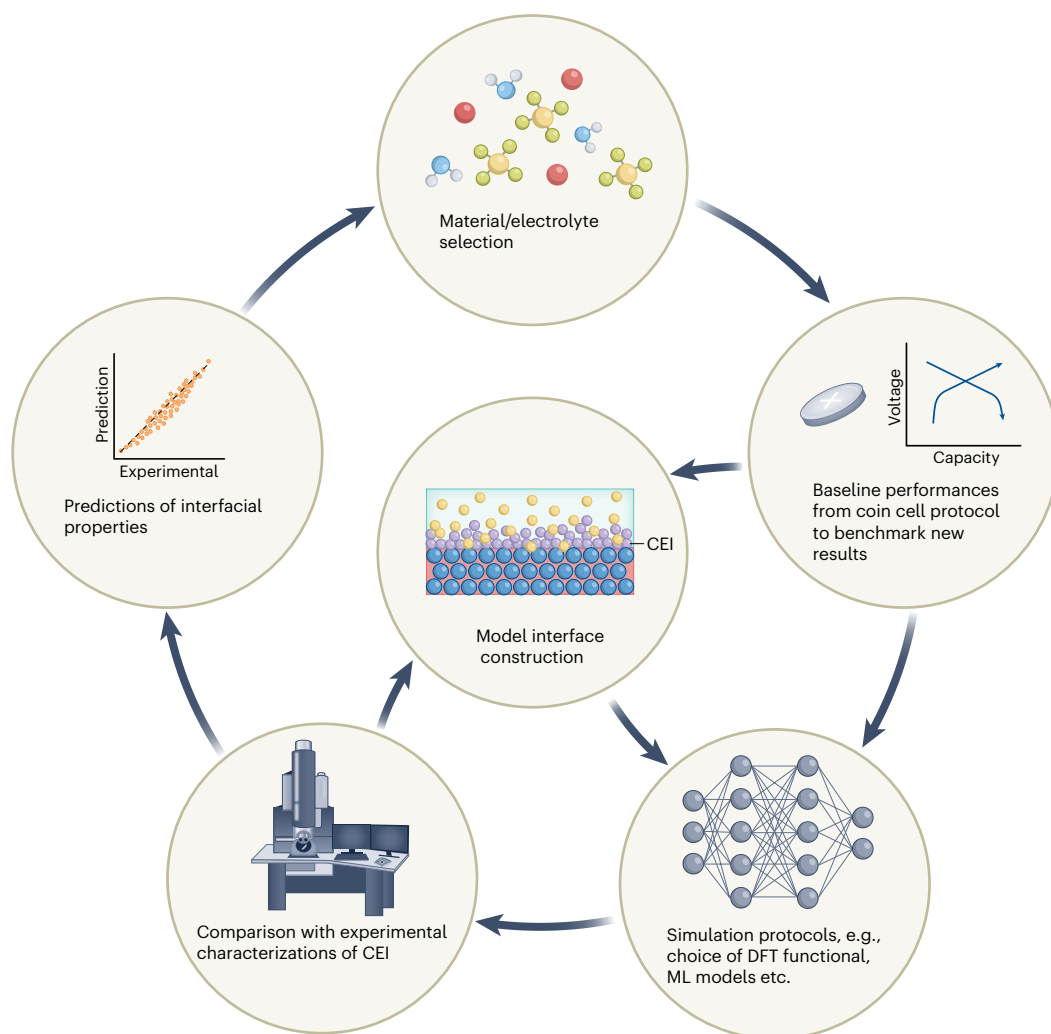


Fig. 4 | An approach for resolving the chemical and structural features of complex electrochemical interphases on the basis of the integration of experiments and theory. Libraries of local interfacial structures and their

associated chemical and structural signatures are constructed and compared against experimentally measured signatures to iteratively refine structural and chemical models.

adding a vast permutation of parameters that impede the isolation of key mechanisms underpinning the reactivity of the electrolyte and cathode material at their interfaces^{67,68}. It is important to note that amounts of carbon additive and binder content are usually very limited in practical cells and about 2% for each to reduce the parasitic weight of the batteries, and therefore impact less on the CEI than on the cathode.

First, due to the sensitive and fragile nature of the CEI, passive and highly sensitive characterization is required to capture its native microstructure and chemistry with minimal damage. For example, TEM could provide atomic scale microstructure and chemical information simultaneously, but the high energy of the electron beam and sample preparation via ion milling or ultramicrotomy will compromise the integrity of the CEI. Beam damage can also occur with synchrotron techniques, such as surface-sensitive soft X-rays. Recent advancements in cryogenic TEM with direct electron detectors and using nanosized particles can help to reduce some of the damage routes of the CEI⁶⁹.

Second, combining techniques that are spatially, laterally or temporally resolved is essential to obtain a more reliable and comprehensive understanding of the CEI. Surface-sensitive techniques, such as X-ray photoelectron spectroscopy, time-of-flight secondary ion mass spectroscopy, soft X-ray absorption spectroscopy and related techniques, have been used to elucidate the chemical distribution of large areas within the CEI. However, they lack sufficient spatial resolution

to resolve the nanostructural species that may develop as a function of exact lateral location on the surface. TEM could resolve the nanoscopic heterogeneity of the CEI, but the size of the field of view that can be measured in reasonable experimental times raises the perennial question of how representative the observations could be^{66,70,71}. This gap could be closed with the use of atomic force microscopy to gain global information on the surface properties of materials or electrodes by rastering large areas with high nanoscale resolution.

Third, real-time monitoring of the CEI dynamic evolution (morphology, composition and fine structure) is critical to understand its role in the electrochemical performance of a battery⁷². As discussed above, in situ/operando experiments should be meticulously designed, benchmarked and optimized. Depending on the specific technique, the in situ set-up may not deliver electrochemical performance (that is, capacity) similar to that from the real cells. However, it should be ensured that the key electrochemical features (oxidation/reduction peaks) are observed so that the information obtained accurately reflects in situ/operando conditions and remains relevant for practical cells.

Fourth, in addition to imaging-based and spectral-based techniques, measurement and in situ monitoring of the properties associated with CEI evolution (for example, ionic conductivity, electrical conductivity and mechanical and thermal response) are also important

to unravel the relationship between CEI components and macroscopic cell behaviour. For example, in situ biasing in TEM was recently applied to measure the electronic conductivity of the SEI, and this was correlated to SEI composition and eventually the electrolyte chemistry⁷³. Scanning electrochemical microscopy, which can give topological information as well as mapping conductivities over a large area, provides another opportunity to correlate CEI components and properties, and eventually the battery performance. While exciting, a critical set of next steps should involve a careful evaluation of the design of the experiment so that the conditions that are analysed approach those in a device, to build real correlations between CEI and cell performance.

Fifth, current understanding and characterization of the CEI mainly focuses on cells at the laboratory scale (that is, coin cells). Moving forward, we suggest charting paths to scale up this understanding to cylindrical or pouch cells, and eventually the pack level under realistic cycling conditions, which will bring the most impactful benefit to industry⁷⁴. Traditional surface analysis techniques are often unable to directly access these buried interphases due to their inaccessible location within the cell. Consequently, developing innovative methods for in situ or operando characterization becomes essential to gain insights into the behaviour and properties of these buried surfaces during cell operation. Fibre/sensor-based devices integrated into such large-format cells could be an effective method to monitor chemical, thermal and molecular-level evolution of battery components⁷⁵.

Finally, in situ/operando experiments generate huge image and spectral datasets. Properly processing and analysing data become time-consuming tasks, which can also introduce artefacts. Combining machine learning (ML), artificial intelligence and advanced characterization techniques could accelerate the data acquisition and analysis in a way that is less labour intensive and reduces human error, while maximizing throughput and automation, which will bring new opportunities for unprecedented progress to solve the pressing challenges in CEI characterization.

Nevertheless, providing unbiased interpretations of such experimental results can be non-trivial. For example, many chemical species or local structural motifs that emerge in the CEI present characteristic signals that may differ from those in the bulk. However, this signal disparity may be sufficient to preclude easy detection of them within experiment measurements, which provide non-local ensemble averaged measurements of the interphase. It is also difficult to elucidate the unique contributions of a given species to the CEI formation and function during operation, especially if they are short lived and are not captured by any experimental probes. In this regard, integrating experimental characterization techniques with complementary modelling and simulations at the atomic scale will be highly rewarding, as it will help to establish a comprehensive understanding of CEI formation and function as shown in Fig. 4.

Challenges and opportunities in simulating CEI

Classical molecular dynamics simulations based on empirical representations of interatomic interactions are routinely used to probe interfacial structures and resolve populations of key chemical constituents of the interphase^{76–78}. Although this approach may still be time limited, coupling classical methods with enhanced sampling techniques can enable a more efficient exploration of potential energy surfaces for out-of-equilibrium reactions and processes^{79–81}. The major drawbacks of this approach are the accuracy and transferability of empirical interatomic potentials due to the lack of electronic representation of chemical interactions; these limitations are apparent for even well-parameterized potentials or the more sophisticated class of reactive force fields. To overcome these challenges, force fields based on modern ML that can preserve quantum-level accuracy but at a fraction of the computational cost become increasingly attractive. With the predictive power of molecular dynamics simulations coupled with high-fidelity ML models, it is now possible to survey a wide range

of interfacial atomic arrangements and associated reaction pathways and it is becoming increasingly feasible to track interfacial evolution under relevant experimental conditions^{76,77,82,83}.

A potential caveat of directly applying atomistic-scale simulations to study the CEI is that any resulting prediction derived from these simulations will exhibit a strong dependence on the quality and complexity of the underlying atomic models. Although this practice presents an opportunity to help isolate and to explore individual factors that contribute to the formation and evolution of the CEI and thus allow the elucidation of structure–property relationships at the interface, it lacks the critical emphasis of realism. Specifically, within this framework, it remains challenging to understand the relevance of key structural and chemical features captured in the model in relation to the materials being used in real electrochemical devices.

Therefore, it is highly desirable to integrate modelling and simulation with solid experimental results and advanced characterization approaches for cross-validation. This concept is illustrated partly in Fig. 4. Upon materials selection, baseline measurements can be conducted to inform modelling factors, such as composition, exposed crystallographic facets of the cathode, local charge/discharge states and so on, and to inform the choice of simulation protocols. Due to the potential complications in modelling open-shell transition metal oxides using density functional theory^{84,85}, special care needs to be taken and comprehensive benchmark tests may become necessary for selecting the appropriate level of theory or density functional theory exchange–correlation functionals. This is not only critically important to accurately describe the electronic interaction of the cathode material with electrolyte components and thus to predict the propensities for interfacial degradation, but it is also essential for providing reliable training datasets for the development of advanced ML models. Once the ML potentials are successfully trained and validated, large-scale molecular dynamics simulations with enhanced sampling can be performed to survey the complex interfacial structure, identify kinetically competing reaction pathways and extract key chemical motifs or representative configurations appearing during interfacial evolution or degradation for spectroscopy calculations. These calculated spectroscopy signatures can be directly used to deconvolute the experimental spectra and provide unbiased elucidation of interfacial sensitivity to external stimuli, such as processing and cell cycling conditions^{86–88}. The comparison with experiment will provide feedback to refine simulation models if necessary to ensure that dominant structural and chemical features of interphases are fully captured. On the basis of this well implemented experiment–theory feedback loop, a foundational understanding of CEI formation can be established for the model system built and tested using the aforementioned consistent protocol. Positive or negative impacts brought by additives or coating layers used to modify CEI can be analysed using the same modelling approach to inform design strategies for manipulating the structure and chemistry of CEI to achieve desired performance.

Outlook

Identifying and tackling challenges related to the CEI at scales relevant to industrial applications is crucial for the successful translation of materials innovation from academic research to practical use. A distinct methodology is necessary to investigate CEI fundamentals on this larger scale.

To study the CEI effectively, it is imperative to ensure that observed electrochemical performance is predominantly influenced by the CEI rather than the SEI or other factors. Utilizing a stable anode such as graphite as the counter-electrode and testing electrochemical cells under conditions relevant to practical applications are essential. Employing a coin cell protocol with parameters close to those of realistic batteries is critical for bridging the scientific gap between small-scale button cells and practical batteries, facilitating fair result comparison among researchers.

Using a model cathode material with validated baseline performance obtained through coin cell protocols will effectively benchmark future results after modifying the CEI through surface coating, new electrolytes or additives. It is crucial to select the best-performing baseline, which can be updated and improved over time. Additionally, tuning anions, rather than solvent molecules, may be more effective in tailoring CEI properties, unless specific solvent molecules strongly adsorb on the positive side. More efforts are required to identify compatible electrolytes for high-Ni NMC cathodes, such as NMC90 and beyond, which exhibit instability and only cycle within a narrow electrochemical window due to continuous cathode impedance growth.

Capturing the transient changes in CEI morphology at different timescales and spatial dimensions remains challenging yet highly important. Overcoming challenges such as reducing beam damage on samples and enhancing the relevance of probed images to practical batteries is essential. Cross-validating observed phenomena using various techniques and testing related hypotheses with proposed coin cell protocols could be a potential approach to quickly confirm or refute conclusions drawn from characterizations. Ideally, non-destructive operando characterization tools are needed to directly observe the rapid evolution of CEI in realistic batteries at different scales.

Modelling and simulating CEI properties should begin with understanding those formed in baseline cells and progress to CEI with enhanced properties validated through coin cell protocols. All simulation results based on validated experimental data will be valuable in building a database for the development of advanced ML models to predict more effective electrolyte recipes or surface engineering strategies accurately.

References

- Xu, K. Electrolytes and interphases in Li-ion batteries and beyond. *Chem. Rev.* **114**, 11503–11618 (2014).
- Ohzuku, T., Iwakoshi, Y. & Sawai, K. Formation of lithium–graphite intercalation compounds in nonaqueous electrolytes and their application as a negative electrode for a lithium ion (shuttlecock) cell. *J. Electrochem. Soc.* **140**, 2490 (1993).
- Kautz, D. J. et al. Designing electrolytes with controlled solvation structure for fast-charging lithium-ion batteries. *Adv. Energy Mater.* **13**, 2301199 (2023).
- Zhang, X. et al. Advanced electrolytes for fast-charging high-voltage lithium-ion batteries in wide-temperature range. *Adv. Energy Mater.* **10**, 2000368 (2020).
- Wen, B. et al. Ultrafast ion transport at a cathode–electrolyte interface and its strong dependence on salt solvation. *Nat. Energy* **5**, 578–586 (2020).
- A study that reveals the relationship between desolvation energy and the CEI's interfacial kinetics.**
- Björklund, E. et al. Cycle-induced interfacial degradation and transition-metal cross-over in $\text{LiNi}_{0.8}\text{Mn}_{0.1}\text{Co}_{0.1}\text{O}_2$ -graphite cells. *Chem. Mater.* **34**, 2034–2048 (2022).
- Liu, W. et al. Inhibition of transition metals dissolution in cobalt-free cathode with ultrathin robust interphase in concentrated electrolyte. *Nat. Commun.* **11**, 3629 (2020).
- Zhang, N. et al. Modified cathode–electrolyte interphase toward high-performance batteries. *Cell Rep. Phys. Sci.* **3**, 101197 (2022).
- Xu, J. Critical review on cathode–electrolyte interphase toward high-voltage cathodes for Li-ion batteries. *Nano-Micro Lett.* **14**, 166 (2022).
- Gutierrez, A. et al. Review—Earth-abundant, Mn-rich cathodes for vehicle applications and beyond: overview of critical barriers. *J. Electrochem. Soc.* **170**, 030509 (2023).
- Clément, R. J., Lun, Z. & Ceder, G. Cation-disordered rocksalt transition metal oxides and oxyfluorides for high energy lithium-ion cathodes. *Energy Environ. Sci.* **13**, 345–373 (2020).
- Nelson, K. J. et al. Studies of the effect of high voltage on the impedance and cycling performance of $\text{Li}[\text{Ni}_{0.4}\text{Mn}_{0.4}\text{Co}_{0.2}]\text{O}_2/\text{graphite}$ lithium-ion pouch cells. *J. Electrochem. Soc.* **162**, A1046–A1054 (2015).
- Yan, P. et al. Tailoring grain boundary structures and chemistry of Ni-rich layered cathodes for enhanced cycle stability of lithium-ion batteries. *Nat. Energy* **3**, 600–605 (2018).
- Hu, J. et al. Locking oxygen in lattice: a quantifiable comparison of gas generation in polycrystalline and single crystal Ni-rich cathodes. *Energy Storage Mater.* **47**, 195–202 (2022).
- Bi, Y. et al. Reversible planar gliding and microcracking in a single-crystalline Ni-rich cathode. *Science* **370**, 1313–1317 (2020).
- A study on how to make a single-crystal, nickel-rich cathode more robust and more efficient.**
- Lin, F. et al. Metal segregation in hierarchically structured cathode materials for high-energy lithium batteries. *Nat. Energy* **1**, 15004 (2016).
- Yan, P. et al. Ni and Co segregations on selective surface facets and rational design of layered lithium transition-metal oxide cathodes. *Adv. Energy Mater.* **6**, 1502455 (2016).
- Zhang, J. et al. Interfacial design for a 4.6V high-voltage single-crystalline LiCoO_2 cathode. *Adv. Mater.* **34**, 2108353 (2022).
- Choi, S. H., Son, J.-W., Yoon, Y. S. & Kim, J. Particle size effects on temperature-dependent performance of LiCoO_2 in lithium batteries. *J. Power Sources* **158**, 1419–1424 (2006).
- Zhang, X. et al. Electrolyte regulating toward stabilization of cobalt-free ultrahigh-nickel layered oxide cathode in lithium-ion batteries. *ACS Energy Lett.* **6**, 1324–1332 (2021).
- Jung, R. et al. Effect of ambient storage on the degradation of Ni-rich positive electrode materials (NMC811) for Li-ion batteries. *J. Electrochem. Soc.* **165**, A132–A141 (2018).
- Liu, D. et al. Review of recent development of in situ/operando characterization techniques for lithium battery research. *Adv. Mater.* **31**, 1806620 (2019).
- Borkiewicz, O. J., Wiaderek, K. M., Chupas, P. J. & Chapman, K. W. Best practices for operando battery experiments: influences of X-ray experiment design on observed electrochemical reactivity. *J. Phys. Chem. Lett.* **6**, 2081–2085 (2015).
- Chen, S. et al. Critical parameters for evaluating coin cells and pouch cells of rechargeable Li-metal batteries. *Joule* **3**, 1094–1105 (2019).
- A study that proposed coin cell and pouch cell critical parameters and testing conditions for the battery research community to bridge the gap between fundamental research and practical adoption of new ideas or materials and to expedite their full integration into realistic battery systems.**
- Liu, J. et al. Pathways for practical high-energy long-cycling lithium metal batteries. *Nat. Energy* **4**, 180–186 (2019).
- Xiao, J. et al. Perspective—Electrochemistry in understanding and designing electrochemical energy storage systems. *J. Electrochem. Soc.* **169**, 010524 (2022).
- Hu, J. et al. Achieving highly reproducible results in graphite-based Li-ion full coin cells. *Joule* **5**, 1011–1015 (2021).
- Bi, Y. et al. Highly stable Ni-rich layered oxide cathode enabled by a thick protective layer with bio-tissue structure. *Energy Storage Mater.* **24**, 291–296 (2020).
- Lu, D. et al. Enabling high-energy-density cathode for lithium–sulfur batteries. *ACS Appl. Mater. Interfaces* **10**, 23094–23102 (2018).
- Xiao, J. Understanding the lithium sulfur battery system at relevant scales. *Adv. Energy Mater.* **5**, 1501102 (2015).
- Zhang, N. et al. Long-term cycling and mechanisms of cell degradation of single crystal $\text{LiNi}_{0.95}\text{Mn}_{0.04}\text{Co}_{0.01}\text{O}_2/\text{graphite}$ cells. *J. Electrochem. Soc.* **171**, 010520 (2024).

32. Bi, Y., Li, Q., Yi, R. & Xiao, J. To pave the way for large-scale electrode processing of moisture-sensitive Ni-rich cathodes. *J. Electrochem. Soc.* **169**, 020521 (2022).
33. Cao, X. Important factors for the reliable and reproducible preparation of non-aqueous electrolyte solutions for lithium batteries. *Commun. Mater.* **4**, 10 (2023).
34. Klein, S. et al. Suppressing electrode crosstalk and prolonging cycle life in high-voltage Li ion batteries: pivotal role of fluorophosphates in electrolytes. *ChemElectroChem* **9**, e202200469 (2022).
35. Zhang, X., Cui, Z. & Manthiram, A. Insights into the crossover effects in cells with high-nickel layered oxide cathodes and silicon/graphite composite anodes. *Adv. Energy Mater.* **12**, 2103611 (2022).
36. Wu, Q., McDowell, M. T. & Qi, Y. Effect of the electric double layer (EDL) in multicomponent electrolyte reduction and solid electrolyte interphase (SEI) formation in lithium batteries. *J. Am. Chem. Soc.* **145**, 2473–2484 (2023).
37. Cao, X. et al. Optimization of fluorinated orthoformate based electrolytes for practical high-voltage lithium metal batteries. *Energy Storage Mater.* **34**, 76–84 (2021).
38. Yamada, Y. et al. Unusual stability of acetonitrile-based superconcentrated electrolytes for fast-charging lithium-ion batteries. *J. Am. Chem. Soc.* **136**, 5039–5046 (2014).
39. Peljo, P. & Girault, H. H. Electrochemical potential window of battery electrolytes: the HOMO–LUMO misconception. *Energy Environ. Sci.* **11**, 2306–2309 (2018).
40. Dong, T. et al. Electrolyte engineering toward high performance high nickel (Ni \geq 80%) lithium-ion batteries. *Adv. Sci.* **11**, 2305753 (2023).
41. Rinkel, B. L. D., Vivek, J. P., Garcia-Araez, N. & Grey, C. P. Two electrolyte decomposition pathways at nickel-rich cathode surfaces in lithium-ion batteries. *Energy Environ. Sci.* **15**, 3416–3438 (2022).
42. Wu, Y. et al. High-voltage and high-safety practical lithium batteries with ethylene carbonate-free electrolyte. *Adv. Energy Mater.* **11**, 2102299 (2021).
43. Dai, P. et al. Synergistic effect of dual-anion additives promotes the fast dynamics and high-voltage performance of Ni-rich lithium-ion batteries by regulating the electrode/electrolyte interface. *ACS Appl. Mater. Interfaces* **14**, 39927–39938 (2022).
44. Zhang, J. et al. Multifunctional solvent molecule design enables high-voltage Li-ion batteries. *Nat. Commun.* **14**, 2211 (2023).
45. Lu, D. et al. A self-purifying electrolyte enables high energy Li ion batteries. *Energy Environ. Sci.* **15**, 3331–3342 (2022).
46. Zou, Y. et al. Non-flammable electrolyte enables high-voltage and wide-temperature lithium-ion batteries with fast charging. *Angew. Chem. Int. Ed.* **62**, e202216189 (2023).
47. An, K., Tran, Y. H. T., Kwak, S., Han, J. & Song, S.-W. Design of fire-resistant liquid electrolyte formulation for safe and long-cycled lithium-ion batteries. *Adv. Funct. Mater.* **31**, 2106102 (2021).
48. Wu, C. et al. Thermal runaway suppression of high-energy lithium-ion batteries by designing the stable interphase. *J. Electrochem. Soc.* **168**, 090563 (2021).
49. Hou, J. et al. Thermal runaway of lithium-ion batteries employing flame-retardant fluorinated electrolytes. *Energy Environ. Mater.* **6**, e12297 (2023).
50. Chen, L. et al. High-safety and high-efficiency electrolyte design for 4.6V-class lithium-ion batteries with a non-solvating flame-retardant. *Chem. Sci.* **14**, 1184–1193 (2023).
51. Fang, M. et al. An electrolyte with less space-occupying diluent at cathode inner Helmholtz plane for stable 4.6V lithium-ion batteries. *Angew. Chem. Int. Ed.* **63**, e202316839 (2023).
52. Xu, J. et al. Electrolyte design for Li-ion batteries under extreme operating conditions. *Nature* **614**, 694–700 (2023).
A work that reports an electrolyte design principle to form stable SEI/CEI for high-energy batteries operating under extreme conditions.
53. Jia, H. et al. Toward the practical use of cobalt-free lithium-ion batteries by an advanced ether-based electrolyte. *ACS Appl. Mater. Interfaces* **13**, 44339–44347 (2021).
54. Páez Fajardo, G. J. et al. Synergistic degradation mechanism in single crystal Ni-rich NMC/graphite cells. *ACS Energy Lett.* **8**, 5025–5031 (2023).
55. Li, J., Downie, L. E., Ma, L., Qiu, W. & Dahn, J. R. Study of the failure mechanisms of LiNi_{0.8}Mn_{0.1}Co_{0.1}O₂ cathode material for lithium ion batteries. *J. Electrochem. Soc.* **162**, A1401–A1408 (2015).
56. Jo, M., Park, S.-H. & Lee, H. NaH₂PO₄ as an electrolyte additive for enhanced thermal stability of LiNi_{0.8}Co_{0.1}Mn_{0.1}O₂/graphite batteries. *J. Electrochem. Soc.* **167**, 130502 (2020).
57. Li, J., Li, W., You, Y. & Manthiram, A. Extending the service life of high-Ni layered oxides by tuning the electrode–electrolyte interphase. *Adv. Energy Mater.* **8**, 1801957 (2018).
58. Li, S. et al. 3,3-diethylene di-sulfite (DES) as a high-voltage electrolyte additive for 4.5 V LiNi_{0.8}Co_{0.1}Mn_{0.1}O₂/graphite batteries with enhanced performances. *ChemElectroChem* **8**, 745–754 (2021).
59. Ren, Z. et al. Delicately designed cyano-siloxane as multifunctional additive enabling high voltage LiNi_{0.9}Co_{0.05}Mn_{0.05}O₂/graphite full cell with long cycle life at 50°C. *Adv. Funct. Mater.* **33**, 2302411 (2023).
60. Zhao, W. et al. Extending the high-voltage operation of graphite/NCM811 cells by constructing a robust electrode/electrolyte interphase layer. *Mater. Today Energy* **34**, 101301 (2023).
61. Cheng, F. et al. Tailoring electrolyte enables high-voltage Ni-rich NCM cathode against aggressive cathode chemistries for Li-ion batteries. *Sci. Bull.* **67**, 2225–2234 (2022).
62. Ma, L., Xia, J. & Dahn, J. R. Improving the high voltage cycling of Li[Ni_{0.42}Mn_{0.42}Co_{0.16}]O₂ (NMC442)/graphite pouch cells using electrolyte additives. *J. Electrochem. Soc.* **161**, A2250–A2254 (2014).
63. Xia, J. et al. Study of triallyl phosphate as an electrolyte additive for high voltage lithium-ion cells. *J. Power Sources* **295**, 203–211 (2015).
64. Keefe, A. S., Weber, R., Hill, I. G. & Dahn, J. R. Studies of the SEI layers in Li(Ni_{0.5}Mn_{0.3}Co_{0.2})O₂/artificial graphite cells after formation and after cycling. *J. Electrochem. Soc.* **167**, 120507 (2020).
65. Thompson, L. M. et al. Quantifying changes to the electrolyte and negative electrode in aged NMC532/graphite lithium-ion cells. *J. Electrochem. Soc.* **165**, A2732–A2740 (2018).
66. Thomas, M. G. S. R., Bruce, P. G. & Goodenough, J. B. AC impedance analysis of polycrystalline insertion electrodes—application to Li_{1-x}CoO₂. *J. Electrochem. Soc.* **132**, 1521–1528 (1985).
67. Demeaux, J., Caillon-Caravanier, M., Galiano, H., Lemordant, D. & Claude-Montigny, B. LiNiMnO/electrolyte and carbon black/ electrolyte high voltage interfaces: to evidence the chemical and electronic contributions of the solvent on the cathode–electrolyte interface formation. *J. Electrochem. Soc.* **159**, A1880–A1890 (2012).
68. Gauthier, M. et al. Electrode–electrolyte interface in Li-ion batteries: current understanding and new insights. *J. Phys. Chem. Lett.* **6**, 4653–4672 (2015).
69. Zhang, Z. W. et al. Cathode–electrolyte interphase in lithium batteries revealed by cryogenic electron microscopy. *Matter* **4**, 302–312 (2021).

70. Huang, W., Wang, H., Boyle, D. T., Li, Y. Z. & Cui, Y. Resolving nanoscopic and mesoscopic heterogeneity of fluorinated species in battery solid–electrolyte interphases by cryogenic electron microscopy. *ACS Energy Lett.* **5**, 1128–1135 (2020).
71. Hestenes, J. C. & Marbella, L. E. Beyond composition: surface reactivity and structural arrangement of the cathode–electrolyte interphase. *ACS Energy Lett.* **8**, 4572–4596 (2023).
72. Lu, J., Wu, T. P. & Amine, K. State-of-the-art characterization techniques for advanced lithium-ion batteries. *Nat. Energy* **2**, 17011 (2017).
A review that summarizes the application of advanced characterization techniques for lithium-ion batteries.
73. Xu, Y. et al. Direct in situ measurements of electrical properties of solid–electrolyte interphase on lithium metal anodes. *Nat. Energy* **8**, 1345–1354 (2023).
74. Xiao, J., Shi, F. F., Glossmann, T., Burnett, C. & Liu, Z. From laboratory innovations to materials manufacturing for lithium-based batteries. *Nat. Energy* **8**, 329–339 (2023).
A Perspective, which reviews challenges and opportunities in scaling up lithium-based battery materials and components to accelerate future low-cost battery manufacturing.
75. Huang, J. Q., Boles, S. T. & Tarascon, J. M. Sensing as the key to battery lifetime and sustainability. *Nat. Sustain.* **5**, 194–204 (2022).
76. Yao, N., Chen, X., Fu, Z. & Zhang, Q. Applying classical, ab initio, and machine-learning molecular dynamics simulations to the liquid electrolyte for rechargeable batteries. *Chem. Rev.* **122**, 10970–11021 (2022).
77. Tan, X. et al. Decoding electrochemical processes of lithium-ion batteries by classical molecular dynamics simulations. *Adv. Energy Mater.* **14**, 2400564 (2024).
78. Kim, S., van Duin, A. C. T. & Shenoy, V. B. Effect of electrolytes on the structure and evolution of the solid electrolyte interphase (SEI) in Li-ion batteries: a molecular dynamics study. *J. Power Sources* **196**, 8590–8597 (2011).
79. Alzate-Vargas, L. et al. Insight into SEI growth in Li-ion batteries using molecular dynamics and accelerated chemical reactions. *J. Phys. Chem. C* **125**, 18588–18596 (2021).
80. Gao, H. et al. Enhanced electrolyte transport and kinetics mitigate graphite exfoliation and Li plating in fast-charging Li-ion batteries. *Adv. Energy Mater.* **13**, 2202906 (2023).
81. Holoubek, J. et al. Predicting the ion desolvation pathway of lithium electrolytes and their dependence on chemistry and temperature. *J. Phys. Chem. Lett.* **13**, 4426–4433 (2022).
82. Diddens, D. et al. Modeling the solid electrolyte interphase: machine learning as a game changer? *Adv. Mater. Interfaces* **9**, 2101734 (2022).
A review that summarizes recent advances in the integration and application of physics-based modeling and ML to the study of solid electrolyte interphases in lithium-ion batteries.
83. Shao, Y., Knijff, L., Dietrich, F. M., Hermansson, K. & Zhang, C. Modelling bulk electrolytes and electrolyte interfaces with atomistic machine learning. *Batter. Supercaps* **4**, 585–595 (2021).
84. Saritas, K., Fadel, E. R., Kozinsky, B. & Grossman, J. C. Charge density and redox potential of LiNiO₂ using ab initio diffusion quantum Monte Carlo. *J. Phys. Chem. C* **124**, 5893–5901 (2020).
85. Timrov, I., Aquilante, F., Cococcioni, M. & Marzari, N. Accurate electronic properties and intercalation voltages of olivine-type Li-ion cathode materials from extended Hubbard functionals. *PRX Energy* **1**, 033003 (2022).
86. Sun, W. et al. Coupled experimental–theoretical characterization of a carbon electrode in vanadium redox flow batteries using X-ray absorption spectroscopy. *ACS Appl. Mater. Interfaces* **16**, 8791–8801 (2024).
A study that demonstrates tight experiment–theory integration for resolving the impact of electrode surface chemistry on electrochemical cell performance.
87. Tamura, T., Kohyama, M. & Ogata, S. Combination of first-principles molecular dynamics and XANES simulations for LiCoO₂–electrolyte interfacial reactions in a lithium-ion battery. *Phys. Rev. B* **96**, 035107 (2017).
88. Carlier, D. et al. DFT+*U* calculations and XAS study: further confirmation of the presence of CoO₅ square-based pyramids with IS-Co³⁺ in Li-overstoichiometric LiCoO₂. *J. Phys. Chem. C* **117**, 26493–26500 (2013).
89. Xiao, J. *Cathode–Electrolyte Interphase (CEI) Consortium: Model Cathode Materials for Next-Generation Li-Ion Batteries* Annual merit review meeting (US Department of Energy Vehicle Technology Office, 2024).
90. Bi, Y. et al. Simultaneous single crystal growth and segregation of Ni-rich cathode enabled by nanoscale phase separation for advanced lithium-ion batteries. *Energy Storage Mater.* **62**, 102947 (2023).

Acknowledgements

This work was supported by the Assistant Secretary for Energy Efficiency and Renewable Energy, Office of Vehicle Technologies of the US Department of Energy (DOE) through the Cathode–Electrolyte Interphase (CEI) Consortium. Pacific Northwest National Laboratory (PNNL) is operated by Battelle for the DOE under contract DE-AC05-76RL01830. Part of the work was performed under the auspices of the US DOE by Lawrence Livermore National Laboratory under contract DEAC52-07NA27344. Sandia National Laboratories is a multi-mission laboratory managed and operated by National Technology and Engineering Solutions of Sandia LLC, a wholly-owned subsidiary of Honeywell International Inc., for the US DOE's National Nuclear Security Administration under contract DE-NA-0003525.

Competing interests

The authors declare no competing interests.

Additional information

Correspondence and requests for materials should be addressed to Jie Xiao.

Peer review information *Nature Energy* thanks Yang-Kook Sun and the other, anonymous, reviewer(s) for their contribution to the peer review of this work.

Reprints and permissions information is available at www.nature.com/reprints.

Publisher's note Springer Nature remains neutral with regard to jurisdictional claims in published maps and institutional affiliations.

Springer Nature or its licensor (e.g. a society or other partner) holds exclusive rights to this article under a publishing agreement with the author(s) or other rightsholder(s); author self-archiving of the accepted manuscript version of this article is solely governed by the terms of such publishing agreement and applicable law.

© Springer Nature Limited 2024